INTEGRATION OF UAV-LIDAR AND UAV-PHOTOGRAMMETRY FOR INFRASTRUCTURE MONITORING AND BRIDGE ASSESSMENT

INTEGRATION OF UAV-LIDAR AND UAV-PHOTOGRAMMETRY FOR INFRASTRUCTURE MONITORING AND BRIDGE ASSESSMENT

F. Gaspari [1], F. Ioli [1], F. Barbieri [1], E. Belcore [2], L. Pinto [1] *

[1] Dept. of Civil and Environmental Engineering (DICA), Politecnico di Milano, Milan, Italy – (federica.gaspari, francesco.ioli, federico2.barbieri, livio.pinto)@polimi.it
[2] Department of Environment, Land and Infrastructure Engineering (DIATI), Politecnico di Torino, Turin, Italy – elena.belcore@polito.it

Commission WG II/10

KEY WORDS: UAV-LiDAR, UAV-photogrammetry, Bridges, Remote inspections, Digital twins, Bridge Monitoring System (BMS).

ABSTRACT:
The health assessment of strategic infrastructures and bridges represents a critical variable for planning appropriate maintenance operations. The high costs and complexity of traditional periodical monitoring with elevating platforms have driven the search for more efficient and flexible methods. Indeed, recent years have seen the growing diffusion and adoption of non-invasive approaches consisting in the use of Unmanned Aerial Vehicles (UAVs) for applications that range from visual inspection with optical sensors to LiDAR technologies for rapid mapping of the territory. This study defines two different methodologies for bridge inspection. A first approach involving the integration of traditional topographic and GNSS techniques with TLS and photogrammetry with cameras mounted on UAV was compared with a UAV-LiDAR method based on the use of a DJI Matrice 300 equipped with a LiDAR DJI Zenmuse L1 sensor for a manual flight and an automatic one. While the first workflow resulted in a centimetric accurate but time-consuming model, the UAV-LiDAR resulting point cloud's georeferencing accuracy resulted to be less accurate in the case of the manual flight under the bridge for GNSS signal obstruction. However, a photogrammetric model reconstruction phase made with Ground Control Points and photos taken by the L1-embedded camera improved the overall accuracy of the workflow, that could be employed for flexible low-cost mapping of bridges when medium level accuracy (5-10 cm) is accepted. In conclusion, a solution for integrating interactively final 3D products in a Bridge Management System environment is presented.

1. INTRODUCTION

Periodical monitoring of strategic infrastructures and bridges is critical for assessing their health and planning adequate maintenance operations. Traditional bridge monitoring techniques often require the adoption of in-situ technical tests with highly expensive dedicated engines. These do not always represent flexible and reproducible solutions. Inspections of road network structures like bridges are traditionally carried out by visual observation and reporting. Similar operations require the support of periodical technical in-situ surveys with elevating platforms and underbridge units or the definition of fixed image-based monitoring systems (Metni & Hamel, 2007). While the first group of operations is subjected to injuries and risks for operators, remote surveillance systems can be considered as a safer option. However, these techniques, though implementing non-invasive approaches, do not always represent flexible and reproducible solutions under different conditions. Fixed-angle cameras installed on the structure combined with 360-degrees optical devices mounted on moving vehicles on top of the bridge are affected by several limitations like visual obstructions (Chen et al., 2019).
In recent years, Unmanned Aerial Vehicles (UAVs) have paved the way for low-cost non-destructive tests for bridge inspections and monitoring (Pinto et al., 2020). Innovative techniques represent valid alternatives compared to less safe and more expensive traditional methods, especially under extreme conditions (Belcore et al., 2021). Then, UAV-based methodologies, supported by organised flight and survey plan, represent a remarkable source of information and data to be integrated or combined with conventional instrumentation in traditional workflows. Visual imaging techniques adopting optical cameras represent the most common Non-Destructive Testing (NDT) approaches for bridge monitoring (Feroz & Abu Dabous, 2021). Other most common methods involve technologies from the field of Infrared Thermography (IRT) and Light Detection and Ranging (LiDAR). This thematic and technical complexity of UAV type of data – analysed as stand-alone products or jointly processed with other data sources - allows exploring multiple possibilities of engineering solutions, involving different expertise and approaches in the workflow. Indeed, the interest in the use of UAV systems in bridge monitoring led to a wide spectrum of studies, ranging from general visual inspection to automatic crack detection (Liu et al., 2016, Dorafshan et al., 2019), including geometric measurement and defect quantification (Adhikari et al., 2014, Kim et al., 2017). Consequently, each type of application requires a dedicated methodology and suitable equipment. UAVs equipped with optical sensors enable the acquisition of images that can be then processed using photogrammetric techniques. Structure from Motion (SfM) (Westoby et al., 2012) processes allow reconstructing 3D scenes of the inspected infrastructure and the surrounding environment, producing scaled digital models that can then be analysed and evaluated for crack or damage detection too. Indeed, this type of application raises important discussions on the geometrical accuracy of the model, which derives directly from the original images acquired in the field (Chen et al., 2017). For this reason, the resolution of the camera mounted on board

* Corresponding author

plays a critical role in the general quality of the process. Apart from this aspect, which also affects the cost of the equipment, high-resolution cameras have been shown to provide efficient outputs for damage identification on structural elements of the bridge (Seo et al., 2018). Hence, the case study peculiarities and the stakeholders' requests for the survey should be carefully considered when defining a procedure. Then the possibility of retrieving remotely visual observation in less accessible areas with significant surveying-time reduction must also be compared with the need for more expensive equipment.

In recent years, thanks to widespread diffusion and significant technological improvements, the use of UAV-based laser scanning for rapid mapping has significantly increased (Nex et al., 2022). Early research was mainly focused on UAV laser scanner applications for forest mapping, biomass quantification and classification (Jaakkola et al. 2010, Wallace et al., 2012). Later, the improvements on the most relevant technological challenges of UAV-LiDAR, such as products georeferencing, sensor and vehicle weight, flight time and instrument calibration, led to a wider variety of studies, also thanks to the cost reduction (Lemmetti et al., 2021). However, the potential of these techniques in infrastructure still needs to be broadly explored. Regardless of the technology adopted, the products resulting from the survey could then consist of technical drawings as well as more dynamical interactive solutions, such as Bridge Monitoring System (BMS) models (Hudson et al., 1987) that could be built upon a wide variety of technologies, integrating Geographic Information (GIS), Building Information Modeling (BIM), web graphic libraries and more technologies.

This work illustrates the definition of two possible methodologies for a bridge monitoring procedure: a traditional and widely established approach that integrates topographic techniques, GNSS, drone-photogrammetry and Terrestrial Laser Scanner (TLS) and an innovative workflow that employs state-of-the-art UAV-based LiDAR for fast acquisition of georeferenced 3D models of bridges with dedicated tests.

The two methods were compared against each other, addressing their main advantages and limitations for their application in bridge inspections, data processing and final products delivery. Moreover, the paper aims at presenting a structured workflow starting from preliminary operations up to the restitution of a digital twin to be included in a web-based Bridge Management System (BMS).

2. THE METHOD

The two methodologies and their related steps were defined as follows:

1. the traditional approach (TRAD) was built on the topographic reference network materialization and measurements, the TLS scans, and the photogrammetric survey;
2. the innovative workflow (UAV-LiDAR) consisted of a LiDAR-equipped drone survey with laser acquisitions and photogrammetric processing of images acquired by the UAV.

Eventually, both methods resulted in an additional phase dedicated to final products preparation for the comparison tests as well as for the delivery to the inspection committers.

2.1 Traditional method

2.1.1 Topographic reference network materialization, measurements, and TLS scans

The application of the traditional method requires that a network, adjusted by least-squares, is materialized in a local reference system in order to avoid cartographic deformation errors.

The first field operation is an inspection of the area to evaluate the optimal number and dislocation of the topographic network nodes and GCPs. Also, the presence of obstacles and all the factors that could lead to problems in the survey activities (for example, high vegetation, amount of traffic, slope of the banks) must be investigated.

The topographic network is materialized by using a total station to measure distances and angles, while an instrument with high precision TLS capacity (<1cm for scans) is adopted for the scanning procedure and the point cloud acquisition.

The network consists of the measurement stations from which a set of targets (used as GCPs in the photogrammetric block and CPs for both TLS and UAV-LiDAR scans in the other surveys) were measured. This allows to create photogrammetric and terrestrial laser datasets in the same reference system, simplifying the following integration and quality comparison.

Then, the referencing of the survey data in a global system is computed through a roto-translation based on 3-5 targets, whose coordinates are measured both in local and global systems, by using a topographic-grade GNSS receiver. The coordinates are acquired in NRTK mode, relying on a permanent GNSS stations network, and lead to 2cm (planimetric) and 3cm (altimetric) accuracy (Ioli, et al., 2021). The TLS dataset is directly generated in the chosen global system.

Due to its high quality, the point cloud acquired by the TLS scanner is considered the reference dataset. Hence, the planning of the scanning points position should guarantee a complete coverage of the structure itself. Typically, 2 or 3 stations are sufficient (at least one on each side of the bridge on the riverbed and one – if possible - above the road path), but this amount could increase depending also on the dimensions and complexity of the structure (height, length, number of spans etc.). A suitable spatial resolution can be obtained by setting the scan grid step of 3-2 cm dimensions for the entire bridge and 2-1 cm for structural elements of interest.

2.1.2 Photogrammetric survey

The photogrammetric survey can be carried out using UAVs that correspond to precise characteristics. First, they must be multi-rotor drones, easy to handle even in manual flight mode; then, they must be equipped with a high-definition digital camera mounted on a gimbal; finally, they must have the possibility to perform automatic flights, planned using specific photogrammetric acquisition software. The proposed acquisition method consists in dividing the aerial survey into two blocks. The first is a nadiral flight, useful for acquiring images of the whole bridge structure and the terrain morphology. It can be planned through a dedicated flight planning software, which allows setting a priori the main photogrammetric parameters, such as overlaps and GSD (Ground Sampling Distance, pixel footprint on the terrain). For the nadiral block, 1-2 cm is generally a suitable value for GSD. The second block consists in a manual flight, in which the lateral elements of the structure (such as piers, abutments, spans and lower parts of the deck) are surveyed. This block comprises images taken from different angles and with sub-centimetric GSD, resulting in a denser point cloud than the terrestrial laser scanner clouds. The two image blocks are processed simultaneously by a traditional SfM (Westoby et al., 2012) with a photogrammetric processing software.

A set of GCPs must be distributed uniformly along the area and the structure surfaces, both the horizontal (road path, terrain on

the abutments, riverbed) and the vertical ones (pillars, guards). Their coordinates are obtained by a total station within the local reference system, materialized as described in Section 2.1.1. The presence of images at different scales and inclinations results in a solid acquisition geometry (James et al., 2020). Therefore, it is possible to carry out a self-calibration of camera interior parameters directly in the Bundle-Block Adjustment (BBA), possibly starting from initial values obtained with in-situ field calibrations (Ioli, et al., 2021) or with a checkerboard (Zhang, 2000). The quality of the BBA should be assessed by using a certain number of GCPs (typically 20-30%, homogeneously distributed on the area and the structure elements) as Check Points (CPs), not used for solving the BBA. Finally, the photogrammetric dense point cloud can be computed and exported for further analysis. A further processing step is the comparison of the resulting point cloud with the one computed with the TLS data for quality assessment. Once verified the coherence of the two different products, a merged point cloud is created.

2.2 UAV-LiDAR survey

LiDAR technology can return highly accurate 3D data even under complex survey conditions, such as unfavourable lighting, in which optical sensors are generally less efficient. This technology, combined with other sensors, can be mounted on aerial vehicles to return reliable 3D measures. The potentials of the joint use of UAV-LiDAR technologies still need to be broadly evaluated, in particular for bridge inspections. Indeed, this type of infrastructures and their designs provide technical challenges that need to be tested, investigating possible limitations of the techniques as well as advantages such as less time-consuming practices for both data acquisition and processing.

Currently, new UAV-LiDAR sensors have entered the market at a comparatively low cost. One of these is the lightweight and affordable LiDAR DJI Zenmuse L1. Along with the DJI Matrice 300 UAV and the proprietary DJI Terra software, this is a complete and integrated system for 3D data acquisition (figure 1). The L1 sensor is mounted on a stabilized 3-axis gimbal and equipped with a built-in RTK GNSS and IMU system for precise georeferencing of the point clouds. Also, it has an integrated RGB sensor that is used to colour the clouds. The optical sensor is a 20 MPx 1" CMOS sensor with a global shutter and a focal length of 8.8 mm. The manufacturer declared a global precision of the LiDAR system of 10 cm in planimetry and 5 cm in height when flying at 50 m AGL and with a constant flying speed of 10 m/s. It supports three reflection returns maximum with the limit of 480.000 points/s for multi-return acquisitions and 240.000 points/s for single return. Štroner et al. (2021) tested the DJI Zenmuse L1 sensor at full-scale. Their analyses showed that the positioning accuracy is better than the manufacturer-declared one: 3.5 cm in all directions versus 10/5 cm horizontal/vertical. Still, the colour information evaluation revealed a systematic shift of approximately 0.2m.

Figure 1. DJI Matrice 300 and DJI Zenmuse P1 camera.

The raw data are collected in a DJI proprietary format and can be processed and converted on standard 3D data formats only using the DJI Terra software. The raw data processing is straightforward and linear, leaving little flexibility to the analyst. The parameters that can be defined include reconstruction density (low, medium, high), the optimization of the accuracy (Yes/No), the output format, and the reference system. Also, it is possible to convert the heights from above the ellipsoid to above the geoid using the global and local model grids. There is no possibility of uploading other grids, but a fixed height offset can be specified.

2.3 Final products preparation and rendering

The processing phases for the photogrammetric, LiDAR and TLS-derived data result in a collection of technical high-quality products. The 3D model reconstruction of the bridge implies the generation of a point cloud that, once filtered and classified, is used as input to produce the mesh, the Digital Terrain Model (DTM) and the orthomosaics (for example, one with a nadiral view and two for the bridge prospects).

Based on these elements, technical drawings may be realized. In particular, the adoption of a Computer-Aided Design (CAD) software makes possible to produce drawings of the bridge facades and deck, as well as accurate cross-sectional illustrations in correspondence of portions of interest, such as abutments or piles using as reference the point cloud. Moreover, in the drawing phase, starting from observations of the drones' images and the point cloud, deteriorated elements can be detected and graphically reported. Hence, the graphical outputs are attached to a technical report that includes in detail the description of the activities carried out, the results obtained and critical considerations on the inspected structure.

Figure 2. Example of a web-based interactive platform for exploring 3D products with oriented images developed with Potree solution.

Alongside the delivery of the final document, the drawings and the point cloud, a web-based digital twin is developed and provided to the commissioners. A possible reproducible solution is Potree (Schutz, 2015), a webGL for interactively viewing large point clouds (Figure 2). Being hosted online, the model could be easily integrated in a dedicated BMS. The chosen technology should make the final 3D products accessible to non-technical end-users through the integration of intuitive and interactive user interface and commands. In this way, it is possible to dynamically navigate through the point clouds and the perspective views derived from oriented images. Additionally, some interactive platforms could implement advanced operations such as direct measurements of distances, angles, areas and volumes or cross sections tracing, also allowing the export of quantitative results.

3. THE CASE STUDY

The two described methodologies were adopted for a masonry single-span bridge in Cortemaggiore (PC, Italy), as part of a series of inspections commissioned by the Piacenza Province.

The process was articulated in two days, the first was dedicated to the TRAD approach while the remaining one was entirely focused on testing the UAV-LiDAR technologies.
In a preliminary phase, a first visual inspection of the area in which the structure is located was conducted remotely using available satellite and street-view imagery (Google and Bing satellite, Google StreetView). This initial exploration of the area helped to define the geographical context of the bridge qualitatively, evaluating its proximity to possible sensitive elements like residential areas and airports. Therefore, information retrieved in this step was crucial not exclusively to understand how to reach the location but also for planning the UAV survey, depending on the classification of the area according to Italian Civil Aviation Authority regulations that outline the flight requirements. The conditions of the bridge were examined through the on-site preliminary inspection that helped identify bushes and creepers that partially covered one of the bridge's abutments (Figure 3). The intrusive vegetation was then properly removed.

Figure 3. Survey site conditions in the preliminary inspection.

3.1 Traditional method application

The information acquired during the preliminary survey – rough estimation of bridge dimensions and identification of obstruction elements - was used for the planning of the topographic network materialized using a Leica Nova Multistation MS60. This instrument can be employed both as a total station and as a high precision laser scanner (<5mm for distances, <1cm for scans, (Fagandini et al., 2017). Moreover, the instrument is equipped with a coaxial high-resolution camera which allows associating RGB information to the scans. The network consisted of 2 station points located on opposite sides of the bridge, ensuring a complete view of the structure (1000, 2000 in Figure 4), used to define the set and the orientation of the local coordinates system. Initially, 16 targets were used, 11 of which were positioned on the bridge: 4 on each side of the structure and 3 under the bridge. This group consisted of 20x20cm Agisoft Metashape (Agisoft, 2021) specific coded targets, which the software can automatically recognise, significantly speeding up the following detection process. The remaining 5 were equally placed in groups of 2 downstream and upstream on the ground and 1 over the bridge in order to be clearly visible in the nadiral pictures. This last group of markers, made of 50x50 cm corex cross targets, was measured with the GNSS receiver Leica Viva GS14 and later used in post-processing for the roto-translation in the global reference system (ETRF2000 (2008) with UTM Zone 32N projection). The limitations in this stage were mainly linked to the riverbed consistency and the need to identify robust and safe positions for the targets on the ground.
The measurements of the topographic network were made using the multistation, as illustrated in Figure 4. The TLS scans were then executed from points 1000 and 2000, defining with the instrument the polygonal views to be used as perimeters for the scanning operation. Several scanning sessions were defined in order to adopt a suitable mean distance value for each portion of the bridge, adopting 3x2 cm as the minimum grid size.
A DJI Mavic Pro 2 drone, equipped with a 1' CMOS sensor with 24 MPx and a focal length of 8.8 mm, was used to collect images. During the first survey, 2 UAV flights were planned and executed with a mean GSD equal to 4 mm, capturing a total amount of 343 photos. The automatic nadiral one was planned using UgCS (UgCS, 2022), a photogrammetric flight planning software.

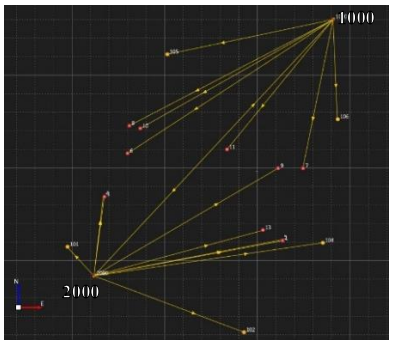

Figure 4. Topographic network, with the two measurement stations 1000 and 2000, and the measured targets.

After the in-situ survey, the topographic network was adjusted by least squares method using the Leica Infinity software, orienting the acquired terrestrial laser point clouds in the local coordinate system. In the following processing phase, the UAV-images were processed in the Agisoft Metashape environment, adopting 5 of the original targets as CPs. The geometrical accuracy of the photogrammetric point cloud, was assessed by the set of CPs, resulting in a Root Mean Square Error (RMSE) of 1.7 cm. After the alignment and optimization phase, a maximum error of 2.5 cm was obtained in correspondence to a target positioned on the downstream facade of the right-hand side abutment of the bridge (Figure 3). Considering the orientation of images in which the target was visible, it was possible to understand that the error was due to a bad projective rays intersection geometry, as all the images were taken with similar angles with respect to the object. In fact, to the presence of vegetation near the bridge abutment prevented a good acquisition geometry in that area.
The resulting photogrammetric dense cloud (Figure 5) consisted in $14x10^6$ points and was obtained after applying filters on the point cloud variance and dense cloud confidence statistics (Agisoft, 2021). The points of the final dense cloud were then manually classified as ground, bridge deck, bridge abutments and road surface.

Figure 5. Photogrammetric 3D model of the Cortemaggiore bridge (Piacenza, Italy).

At the same time, the TLS scans were processed in the Leica Infinity environment obtaining a residual georeferencing error of 1 cm along the three local coordinates and a point cloud whose numerosity was equal to $3x10^6$ points (Figure 6). It is necessary to remark that the upper bridge deck portion was missing in the resulting point clouds because it was not visible from either of the two stations. The integration of the TLS and photogrammetric clouds was a crucial step to obtain a complete and robust 3D reconstruction of the bridge model.

Figure 6. TLS point cloud of the Cortemaggiore bridge (Piacenza, Italy).

The photogrammetric accuracy issue was visible also in the point clouds comparison resulting in a RMSE equal to 1.4 cm, in the tolerance range defined by the average Ground Sample Distance. However, by computing the cloud-to-cloud distances in CloudCompare (Girardeau-Montaut, 2016) environment, the significant inconsistencies between the two products were identified only in correspondence to the downstream facade of the right-hand side abutment. The final integrated cloud was then computed by merging the two products, except for the downstream portion, in which only TLS-derived points were kept minimizing the model error. Additionally, the resulting point cloud was referenced into a global reference system by applying a roto-translation based on the GNSS field observations.

3.2 UAV-LiDAR survey

The UAV-LiDAR survey was executed with a DJI Matrice 300, a 6 kg quadcopter ($81\ cm \times 67\ cm \times 43\ cm$) equipped with a GNSS RTK receiver. It can carry payloads up to 2.7 kg, and it has 55 minutes of flight autonomy. The drone is equipped with a L1 Zenmuse LiDAR, designed to be mounted on a UAV of the same manufacturer.
Two flights were performed: a planned flight at an altitude of $35\ m$ (referred to as Automatic LiDAR-AL) and the second in manual piloting at variable height (a Manual LiDAR flight hereafter mentioned as ML). AL was performed with -90° gimbal pitch (nadiral) and a sample rate of 80 kHz, while ML was performed with -30° gimble pitch and 160 kHz sample rate. The speed was set constant to 5 m/s for AL. As suggested by the manufacturer, the scan mode was always set to "repeat", and each acquisition was calibrated (calibration "yes"). The characteristics of the two flights performed are reported in Table 1.

Parameters	AL	ML
Type	Planned	Manual
Overlap	40%	Manually maintained approx. 60%
Height	35	variable
gimbal pitch	-90°	-30°
Speed of flight	5 m/s	Variable, approx. 5 m/s
sample rate	80 kHz	160 kHz
scan mode	repeat	repeat

Table 1. The flights' characteristics

The two acquisitions were processed with DJI Terra in the global system ETRF2000 (2008) with UTM projection, with "high" reconstruction density and optimization of accuracy enabled. The processed clouds were exported in LAS format, storing the RGB and intensity information (Figure 7). Then AL cloud has $1x10^6$ points, while the ML one has $632x10^6$ points.
Unlike AL, ML also provided data from the bottom and the abutments of the bridge by flying at constant speeds under the bridge.

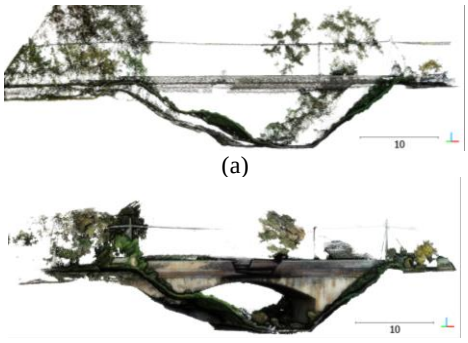

(a)

(b)

Figure 7. The LiDAR point clouds: (a) AL point cloud, (b) ML point cloud

First, the global accuracy of the AL flight was evaluated by calculating the residuals between coordinates values of GCPs measured with the GNSS receiver and extracted from the AL point cloud (Table 2). This validation could not be applied to the ML case because its surveyed area corresponded to the bottom portion of the bridge, where no GCPs were positioned.

	East	North	$h_{ellipsoidal}$
Average (m)	0.07	-0.02	-0.02
σ (m)	0.06	0.09	0.03
$RMS\ (m)$	0.09	0.09	0.04

Table 2. Statistics on the differences for GCPs coordinates between the values calculated with the AL flight and those measured by GNSS receiver.

The overall survey accuracy (RMS) is in the order of 10 cm for the AL flight at 35 m height Above Ground Level (AGL). The inconsistencies can be partially ascribed to a systematic error (deducible from the mean of the differences) that depends on the cloud colouring process and on the georeferencing of the LiDAR survey based on the drone trajectory obtained from GNSS and IMU data. This error is about 5-7 cm. On the other side, the precision of the survey (deducible from the standard deviation σ of the differences) is attested to values that, for the three coordinates, vary between 3 and 9 cm, in accordance with the manufacturer's statements.
The consequent analysis consisted in evaluating the coherence and consistency of the AL and ML flights, identifying possible discrepancies in the resulting point clouds. Then, the clouds acquired on the bridge were merged, and 3 cross-sections of the bridge cloud were computed.
Figure 8 shows the positions of the sections, while Figure 9 illustrates in detail each cross-section made to highlight the differences between the point clouds (Table 3). The computed statistics are again aligned with the ones stated by the manufacturer, with an RMS in the 8-11 cm range.

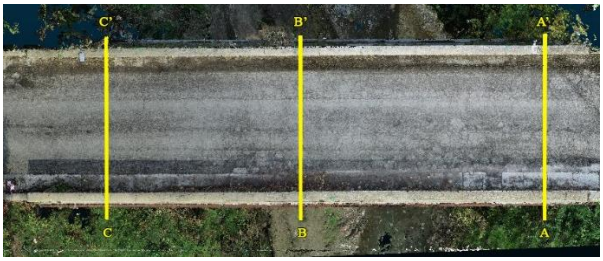

Figure 8. Location of the cross-sections analysed.

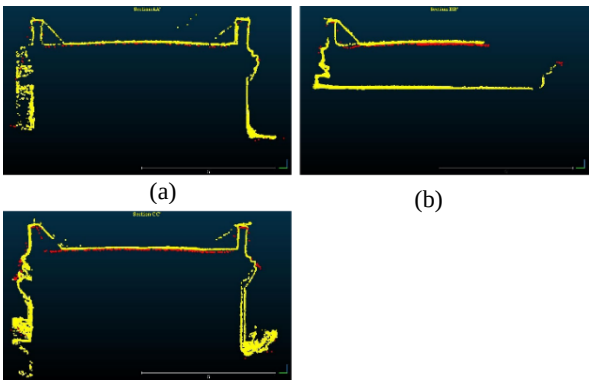

(a) (b) (c)

Figure 9. Comparisons of the cross-sections of AL (red) and ML (yellow) for sections: (a) AA'; (b) BB'; (c) CC'.

Cross-sections	AA'	BB'	CC'
Average (m)	0.06	0.07	0.08
σ (m)	0.04	0.04	0.07
$RMS\ (m)$	0.08	0.08	0.11

Table 3. Statistics on the differences between the AL and ML point clouds for each cross-section.

The cross-section CC' (Figure 9c) shows two different acquisitions of the bridge's right abutment as the result of two distinct passages of the drone under the bridge. It should be noted that for the ML flight in case of lack of GNSS data signal – a common issue especially when flying below bridge decks - the georeferencing of the data loses reliability. The difference between the two acquisitions is about 16 cm. Moreover, the UAV-LiDAR merged point cloud was compared with the photogrammetric and TLS TRAD point cloud using the M3C2 (Lague et al., 2013), and a RMSE of 10.9 cm was obtained (Figure 10), which is in line with the expected accuracy for the RTK GNSS and IMU system used to georeferenced the cloud, also considering the issue reported for the ML flight.

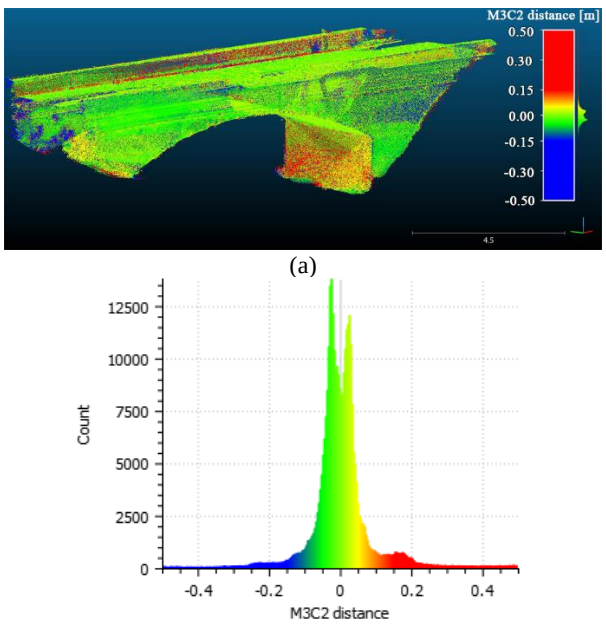

(a) (b)

Figure 10. (a) Distances between the L1 LiDAR point cloud and the TRAD integrated point cloud (computed with the M3C2 algorithm in Cloud Compare). Points with red and blue saturated colours are those with distances exceeding ±15 cm; b) histogram of the differences

Hence, the lower accuracy of the georeferencing of the ML output and the noise of its point cloud raised the need for possible additional data to improve the overall accuracy of the LiDAR survey for infrastructure inspections, especially in the case of bridges. In addition to direct measurements of bridge spans, parapets, heights or roadway widths, the images taken by the UAV-LiDAR optical camera represent an important source of data to be properly investigated with a traditional photogrammetric processing. For this reason, following the previous discussions on the resulting accuracy, the ML+AL product was integrated and updated with the photogrammetric model reconstructed using 172 images collected by the UAV-LiDAR vehicle (Figure 11).

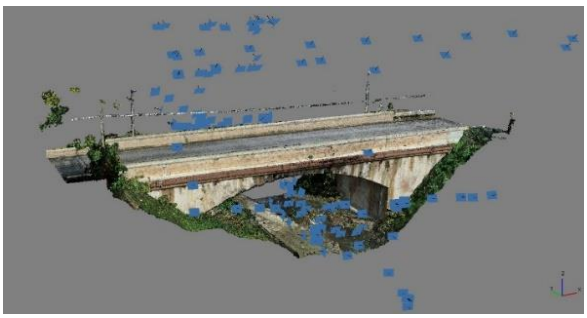

Figure 11. Photogrammetric model reconstructed with images collected during the UAV-LiDAR survey.

The obtained digital twin of the bridge – made of $7x10^6$ points - was characterised by an overall accuracy comparable with the photogrammetric one obtained with the traditional method. Indeed, 5 markers were used for the alignment phase, obtaining a final error of 3 cm on CPs. Then, the point cloud was integrated with the UAV-LiDAR ML and AL product, filtering noises in the CloudCompare environment by applying a SOR filter (with 2 iterations). This led to the removal of the points resulting from the double acquisition on the bottom of the bridge deck. Hence, the UAV-LiDAR integrated cloud was compared to the TRAD integrated one with the M3C2 tool (Figure 12).

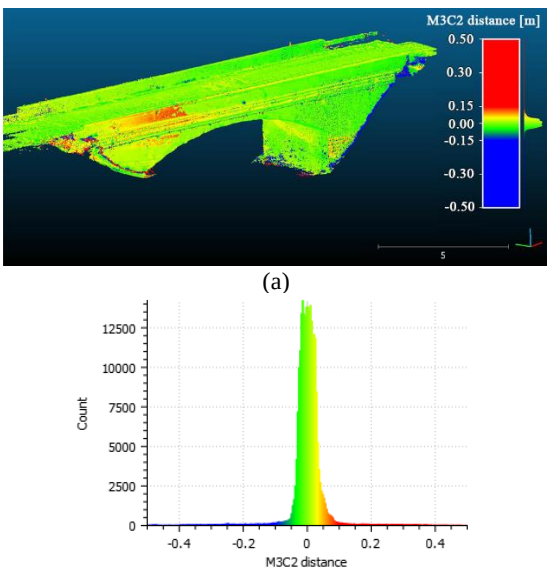

(a) (b)

Figure 12. a) Distances between the UAV-LiDAR integrated point cloud and the TRAD integrated point cloud; b) histogram of the differences

In Figure 12a) it is clearly visible the absence of inconsistencies area depicted in red below the structure. Also, differently from what obtained in Figure 10, the histogram of the differences (Figure 12b) shows how the differences are shaped as a single-headed Gaussian function with an average value of 2 mm and σ of 6,9 cm comparable with the accuracy obtained for the TRAD integrated cloud too.

3.3 Final products

The photogrammetric-TLS dense cloud was used as source material for the generation of a mesh. Hence, three orthophotos (nadiral, upstream and downstream bridge prospects) were realised with 1cm resolution. A $20\ cm \times 20\ cm$ DTM was also calculated starting from the dense cloud, obtaining the contour lines used for the technical drawings realised in AutoCAD. The output of this phase consisted of 3 scaled drawing boards illustrating the planimetry, the prospects and the commissioned cross-sections. In this case, three cross-sections were traced: 2 for the abutments and 1 in correspondence to the arc key. The technical tables also reported indications on the position of portions of the bridge affected by deterioration.
Finally, the interactive 3D platform was implemented to provide the commissioners with an easy-to-use interface that allows non-expert final users to explore 3D data and possibly embed them in a BMS. To this end, the bridge point cloud and the oriented images of the photogrammetric block were rendered and uploaded to a web server with Potree (Schutz, 2015), an open-source web-based graphics library for visualizing large point clouds through a web browser (Figure 12). The integrated point cloud resulting from the merging and subsampling of the photogrammetric and TLS-acquired ones has been converted into an indexed JavaScript Object Notation (JSON) format using PotreeConverter. Hence, the original file could be interpreted and rendered using WebGL technologies on a web server where it is hosted. In this way, the committer and every user who has access to the web page where the Potree model is hosted could investigate the quality of the dense cloud, by dynamically quantifying distances, areas and angles as well as rapidly evaluating cross-sections of the structures.
Additionally, a selection of the oriented drone images could be viewed through a clickable set of icons aligned to the model using the information of the camera calibration certificate and the images' external orientation parameters. Using this solution, the committers had not to download a large amount of data nor install additional technical software to locally explore the point cloud of the bridge. Indeed, the digital twin was hosted online, making possible to easily share the survey results, deriving, through Potree potentialities, additional information that could be saved and exported for planning future maintenance operations in line with national guidelines on the topic.

Figure 13. BMS-embeddable web interface developed with Potree.

4. CONCLUSIONS

The significant presence in the world of bridges in poor conditions highlights the need for systematic low-cost inspections and health assessments. The case study investigated the main advantages and limitations that affect two feasible and reproducible methodologies that consider different techniques with variable costs, flexibility, and applications in infrastructure monitoring. In particular, the traditional approach, employing topographic measurements, UAV-photogrammetry and TLS, obtained more accurate (i.e., centimetric) final 3D products. However, the choice of this method could represent a challenge because of the need for much equipment (UAV+GNSS+total station) and operators' team, usually also resulting in a more expensive, time-consuming workflow in both the survey and processing steps. On the other side, the UAV-LiDAR survey, adopting a limited number of instruments, revealed to be the least time-consuming and expensive technique, despite an overall lower accuracy that could be refined through the integration of an additional photogrammetric process of the images acquired by the L1-embedded camera, highlighting the importance of a robust set of GCPs. Eventually, as discussed in the case study, both methodologies are affected by limitations due to techniques' peculiarities, which can be overcome by integrating data in a post-processing phase.
In conclusion, both the approaches represent valuable alternatives for bridge inspection, with the choice of adoption between them depending on the inspection conditions and committers' requests. The traditional method can provide centimetric accurate solutions. On the contrary, the UAV-LiDAR technique is a valid alternative for moderate accurate (5-10 cm) surveys of bridges. Moreover, in case of a series of structure inspections in a short time range, this technology could also ensure greater flexibility.
Regardless of the choice of the methodology, the comparison and combination of photogrammetric and LiDAR procedures allow for good-quality digital twins of the structure that could be used as a comprehensive reference for planning future interventions and extrapolating technical drawings from accurate and georeferenced 3D data.

REFERENCES

Adhikari, R. S., Moselhi, O., Bagchi, A., 2014. Image-based retrieval of concrete crack properties for bridge inspection. *Automation in construction*, 39: 180-194.

Agisoft, 2021. Agisoft Metashape User Manual - Professional Edition, Version 1.7. https://www.agisoft.com/pdf/metashape-pro_1_7_en.pdf

Belcore, E., Pietra, V. D., Grasso, N., Piras, M., Tondolo, F., Savino, P., Osello, A., 2021. Towards a FOSS Automatic Classification of Defects for Bridges Structural Health Monitoring. In Italian Conference on Geomatics and Geospatial Technologies (pp. 298-312). Springer, Cham.

Chen, S., Laefer, D. F., Byrne, J., & Natanzi, A. S., 2017. The effect of angles and distance on image-based, three-dimensional re-constructions. In *27th annual European Safety and Reliability Conference*, Portoroz, Slovenia, June, 2017. CRC Press.

Chen, S., Laefer, D. F., Mangina, E., Zolanvari, S. I., Byrne, J., 2019. UAV bridge inspection through evaluated 3D reconstructions. *Journal of Bridge Engineering*, 24(4).

Dorafshan S, Thomas RJ, Maguire M., 2019. Benchmarking Image Processing Algorithms for Unmanned Aerial System-Assisted Crack Detection in Concrete Structures. *Infrastructures*. 4(2), 19.

Fagandini, R., Federici, B., Ferrando, I., Gagliolo, S., Pagliari, D., Passoni, D., Pinto, L., Rossi, L., Sguerso, D., 2017. Evaluation of the Laser Response of Leica Nova MultiStation MS60 for 3D Modelling and Structural Monitoring. *Computational Science and Its Applications – ICCSA 2017*, 93–104.

Feroz, S., Abu Dabous, S., 2021. UAV-Based Remote Sensing Applications for Bridge Condition Assessment. *Remote Sensing*, 13(9), 1809.

Girardeau-Montaut, D., 2016. CloudCompare. *France: EDF R&D Telecom ParisTech.*

Hudson, S. W., Carmichael III, R. F., Moser, L. O., Hudson, W. R., Wilkes, W. J., 1987. Bridge management systems. NCHRP Report, (300).

Ioli, F., Pinto, L., Ferrario, F., 2021. Low-cost DGPS assisted aerial triangulation forsub-decimetric accuracy with non-RTK UAVs, *Int. Arch. Photogramm. Remote Sens. Spatial Inf. Sci*., XLIII-B2-2021, 25–32.

Jaakkola, A., Hyyppä, J., Kukko, A., Yu, X., Kaartinen, H., Lehtomäki, M., & Lin, Y., 2010. A low-cost multi-sensoral mobile mapping system and its feasibility for tree measurements. *ISPRS journal of Photogrammetry and Remote Sensing*, *65*(6), 514-522.

James, M.R., Antoniazza, G., Robson, S., Lane, S.N., 2020. Mitigating systematic error in topographic models for geomorphic change detection: accuracy, precision and considerations beyond off-nadir imagery. *Earth Surf. Process. Landforms*, 45, 2251–2271.

Kim H., Ahn E., Cho S., Shin M., Sim S.H., 2017. Comparative analysis of image binarization methods for crack identification in concrete structures, *Cement and Concrete Research*, 99, 53-61.

Lague, D., Brodu, N., & Leroux, J., 2013. Accurate 3D comparison of complex topography with terrestrial laser scanner: Application to the Rangitikei canyon (NZ). *ISPRS Journal of photogrammetry and remote sensing*, 82, 10-26.

Lemmetti, J., Sorri, N., Kallioniemi, I., Melanen, P., Uusimaa, P., 2021. Long-range all-solid-state flash LiDAR sensor for autonomous driving. In *High-Power Diode Laser Technology. XIX* (Vol. 11668, p. 116680P). International Society for Optics and Photonics.

Liu Y.F., Cho S., B. F. Spencer Jr., Fan J.S., 2016. Concrete crack assessment using digital image processing and 3D scene reconstruction. *Journal of Computing in Civil Engineering*, 30(1), 04014124.

Metni, N., Hamel, T., 2007. A UAV for bridge inspection: Visual servoing control law with orientation limits. *Automation in construction*, 17(1), 3-10.

Nex, F., Armenakis, C., Cramer, M., Cucci, D. A., Gerke, M., Honkavaara, E., Skaloud, J., 2022. UAV in the advent of the twenties: Where we stand and what is next. *ISPRS Journal of photogrammetry and remote sensing*, 184, 215-242.

Pinto, L., Bianchini, F., Nova, V., Passoni, D., 2020. Low-Cost UAS Photogrammetry for road Infrastructures'inspection. *Int. Arch. Photogramm. Remote Sens. Spatial Inf. Sci*., XLIII-B2-2020, 1145-1150

Schuetz, M., 2016. Potree: Rendering Large Point Clouds in Web Browsers. Master's thesis, Technische Universitat Wien

Seo, J., Duque, L., Wacker, J., 2018. Drone-enabled bridge inspection methodology and application. *Automation in Construction*, 94, 112-126.

Štroner, M., Rudolf U., Lenka L., 2021. A New Method for UAV Lidar Precision Testing Used for the Evaluation of an Affordable DJI ZENMUSE L1 Scanner. *Remote Sensing* 13(23), 4811.

UgCS, 2022. UgCS Desktop User Manual, https://wiki.ugcs.com/UgCS_desktop_User_Manual

Wallace, L., Lucieer, A., Watson, C., Turner, D., 2012. Development of a UAV-LiDAR system with application to forest inventory. *Remote sensing*, 4(6), 1519-1543.

Westoby, M. J., Brasington, J., Glasser, N. F., Hambrey, M. J., Reynolds, J. M., 2012. 'Structure-from-Motion' photogrammetry: A low-cost, effective tool for geoscience applications. *Geomorphology*, 179, 300-314.

Zhang, Z., 2000. A Flexible New Technique for Camera Calibration. *IEEE Trans. Pattern Anal. Mach. Intell.* 22, 11 (November 2000), 1330 - 1334.